Use of Piezoelectric Shear Response in Adaptive Sandwich Shells of Revolution - Part 2: Finite Element Implementation

Ayech Benjeddou, V. Gorge, Roger Ohayon

Use of Piezoelectric Shear Response in Adaptive Sandwich Shells of Revolution – Part 2: Finite Element Implementation

A.BENJEDDOU, V.GORGE AND R.OHAYON*

Structural Mechanics and coupled systems laboratory, Conservatoire National des Arts et Métiers, 2 rue Conté, 75003 Paris, France

ABSTRACT: A theoretical model has been presented in Part 1 of this paper for the use of piezoelectric shear response in adaptive sandwich shells of revolution. This second part presents its corresponding finite element implementation. For this, an isoparametric finite element discretization is retained for the cylindrical coordinates and independent mechanical and electric variables. These are interpolated with linear Lagrange polynomials along the meridian, but expanded with Fourier series along the shell circumference. This leads to a simple two-nodes conical finite element with 22 degrees of freedom. Straight meridian has been assumed to reduce eventual membrane locking, whereas the selective reduced integration has been used to avoid eventual shear locking. Therefore, prior to the element assembly, a geometric transformation from local curvilinear to global cylindrical coordinate system was made to take into account the shell meridian curvature and to handle its eventual discontinuities. After its validation, the present finite element has been used for vibration analysis of adaptive sandwich cylindrical shells and circular plates with open- and short-circuited embedded piezoelectric shear actuators. It was found that, contrary to extension actuators, shear ones are insensitive to the electric boundary conditions for axisymmetric modes. For non-axisymmetric ones, it was also found that bending modes dependence varies more than other radial, torsion and extension ones.

INTRODUCTION

ALTHOUGH several theoretical analyses have been conducted on the shear response of piezoceramics (Benjeddou et al., 2001), recent bibliography (Mackerle, 1998), literature review (Saravanos and Heyliger, 1999) and survey (Benjeddou, 2000a) have indicated that there are no piezoelectric shell finite elements treating with this feature. Therefore, it is the aim of this part of the paper to present the finite element formulation corresponding to the theoretical one (Benjeddou et al. 2001). For this, a simple conical finite element is proposed. It uses a Fourier series decomposition along the shell circumference and linear Lagrange polynomials along the meridian for all mechanical and electric model variables. Hence, in the following, the stiffness, mass and load element matrices of the axisymmetric sandwich shell element are derived from the discretization of the internal, inertia and external virtual works presented in Part 1 (Benjeddou et al. 2001) of this paper. Then, the vibration problem is derived for validation and applications purpose.

*Author to whom correspondence should be addressed.
E-mail: ohayon@cnam.fr

FINITE ELEMENT DISCRETIZATION

Consider the conical finite element presented in Figure 1. The shell meridian is assumed straight in order to attenuate any eventual membrane locking. It is defined using its radial, r, and axial, Z, cylindrical coordinates discretized linearly as

$$X(s) = N_1(s)X_1 + N_2(s)X_2 \tag{1}$$

with

$$N_1(s) = 1 - s/L, \quad N_2(s) = s/L$$

s is the curvilinear meridian coordinate and L is the element length. X is either of r or Z. X_1, X_2 are their corresponding nodal values.

Mean and relative faces displacements and rotations, core electric potentials and the shell deflection are expanded along the shell circumference using Fourier series as

$$\left\{d(s,\theta)\right\} = \left\{d_0(s)\right\} + \sum_{j=1}^{\infty}\left([t^S(j\theta)]\left\{d_j^S(s)\right\} + [t^A(j\theta)]\left\{d_j^A(s)\right\}\right) \tag{2}$$

with

$$\langle d\rangle = \langle\, \bar{u} \quad \bar{v} \quad w \quad \bar{\beta} \quad \bar{\beta}_\theta \quad \bar{\varphi} \quad \tilde{u} \quad \tilde{v} \quad \tilde{\beta} \quad \tilde{\beta}_\theta \quad \tilde{\varphi} \,\rangle$$

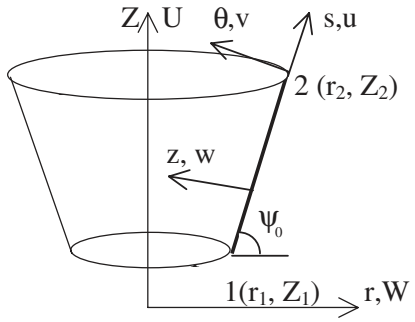

Figure 1. *The conical element: geometry and notations.*

$$[t^s(j\theta) = \mathrm{diag}(\cos(j\theta)\sin(j\theta)\cos(j\theta)\cos(j\theta)\sin(j\theta)\cos(j\theta)\ldots\cos(j\theta)\sin(j\theta)\cos(j\theta)\sin(j\theta)\cos(j\theta))$$

$$[t^A(j\theta) = \mathrm{diag}(\sin(j\theta) - \cos(j\theta)\sin(j\theta)\sin(j\theta) - \cos(j\theta)\sin(j\theta)\ldots\sin(j\theta) - \cos(j\theta)\sin(j\theta) - \cos(j\theta)\sin(j\theta))$$

$\{d_0(s)\}$, $\{d_j^s(s)\}$ and $\{d_j^A(s)\}$ have the same components as $\{d\}$, above, but representing its axisymmetric ($j=0$), symmetric (S) and anti-symmetric (A) Fourier components. It is well known (Benjeddou and Hamdi, 1996) that for free vibrations, symmetric and antisymmetric resulting problems have similar eigenvalues, but opposite sign eigen vectors. Also, for static analyses, a unique problem can be solved, but with symmetric and antisymmetric load vectors. Hence, from now on, only symmetric Fourier series components of the independent variables vector are retained. Also, for simplicity, the Fourier series index j and symmetric S superscript are omitted.

After the Fourier series decomposition along the shell circumference, the model independent variables are interpolated using linear Lagrange polynomials according to Equation (1), where the X variable is either of the components of the vector $\{d_j^s(s)\}$ and X_1, X_2 are their corresponding nodal degrees of freedom (DOF). Since all quantities are decomposed into mean and relative contributions, these are discretized separately using reduced DOF vectors. Hence, the jth harmonic order symmetric components of mean and relative displacements and rotations are discretized along the meridian as

$$\begin{aligned}
\left\{\bar{d}_t(s)\right\} = [N3(s)]\left\{\bar{d}_t^e\right\},\ \left\{\bar{d}_p(s)\right\} &= [N2(s)]\left\{\bar{d}_p^e\right\},\\
\left\{\tilde{d}_p(s)\right\} &= [N2(s)]\left\{\tilde{d}_p^e\right\},\\
\left\{\bar{d}_r(s)\right\} &= [N2(s)]\left\{\bar{d}_r^e\right\},\\
\left\{\tilde{d}_r(s)\right\} &= [N2(s)]\left\{\tilde{d}_r^e\right\}
\end{aligned} \tag{3}$$

with

$$\begin{aligned}
&\langle\bar{d}_t\rangle = \langle\,\bar{u}\quad\bar{v}\quad w\,\rangle,\ \langle\bar{d}_t^e\rangle = \langle\,\bar{u}_1\quad\bar{v}_1\quad w_1\quad\bar{u}_2\quad\bar{v}_2\quad w_2\,\rangle\\
&\langle\bar{d}_p\rangle = \langle\,\bar{u}\quad\bar{v}\,\rangle,\ \langle\bar{d}_p^e\rangle = \langle\,\bar{u}_1\quad\bar{v}_1\quad\bar{u}_2\quad\bar{v}_2\,\rangle\\
&\langle\tilde{d}_p\rangle = \langle\,\tilde{u}\quad\tilde{v}\,\rangle,\ \langle\tilde{d}_p^e\rangle = \langle\,\tilde{u}_1\quad\tilde{v}_1\quad\tilde{u}_2\quad\tilde{v}_2\,\rangle\\
&\langle\bar{d}_r\rangle = \langle\,\bar{\beta}\quad\bar{\beta}_\theta\,\rangle,\ \langle\bar{d}_r^e\rangle = \langle\,\bar{\beta}_1\quad\bar{\beta}_\theta 1\quad\bar{\beta}_2\quad\bar{\beta}_\theta 2\,\rangle\\
&\langle\tilde{d}_r\rangle = \langle\,\tilde{\beta}\quad\tilde{\beta}_\theta\,\rangle,\ \langle\tilde{d}_r^e\rangle = \langle\,\tilde{\beta}_1\quad\tilde{\beta}_\theta 1\quad\tilde{\beta}_2\quad\tilde{\beta}_\theta 2\,\rangle\\
&[N3(s)] = \begin{bmatrix} N_1(s) & 0 & 0 & N_2(s) & 0 & 0\\ 0 & N_1(s) & 0 & 0 & N_2(s) & 0\\ 0 & 0 & N_1(s) & 0 & 0 & N_2(s)\end{bmatrix}\\
&[N2(s)] = \begin{bmatrix} N_1(s) & 0 & N_2(s) & 0\\ 0 & N_1(s) & 0 & N_2(s)\end{bmatrix}
\end{aligned}$$

Substituting these expressions in those of the jth harmonic order symmetric components of the corresponding extension (e), bending (χ) and shear (γ) strains (Benjeddou et al., 2001), provides

$$\begin{aligned}
\{\bar{e}\} &= [B3]\left\{\bar{d}_t^e\right\}, \quad \{\tilde{e}\} = [B2]\left\{\tilde{d}_p^e\right\}\\
\{\bar{\chi}\} &= [B2]\left\{\bar{d}_r^e\right\}, \quad \{\tilde{\chi}\} = [B2]\left\{\tilde{d}_r^e\right\}\\
\left\{\bar{\gamma}\right\} &= [\bar{B}_s]\left\{\bar{d}^e\right\}, \quad \left\{\tilde{\gamma}\right\} = [\tilde{B}_s]\left\{\tilde{d}^e\right\}\\
\left\{\bar{\gamma}^c\right\} &= [\bar{B}_s^c]\left\{\bar{d}^e\right\}, \quad \left\{\tilde{\gamma}^c\right\} = [\tilde{B}_s^c]\left\{\tilde{d}^e\right\}
\end{aligned} \tag{4}$$

with

$$\begin{aligned}
&\langle\bar{d}^e\rangle = \langle\,\bar{u}_1\quad\bar{v}_1\quad w_1\quad\bar{\beta}_1\quad\bar{\beta}_{\theta 1}\quad\bar{u}_2\quad\bar{v}_2\quad w_2\quad\bar{\beta}_2\quad\bar{\beta}_{\theta 2}\,\rangle\\
&\langle\tilde{d}^e\rangle = \langle\,\tilde{u}_1\quad\tilde{v}_1\quad\tilde{\beta}_1\quad\tilde{\beta}_{\theta 1}\quad\tilde{u}_2\quad\tilde{v}_2\quad\tilde{\beta}_2\quad\tilde{\beta}_{\theta 2}\,\rangle
\end{aligned}$$

All strain matrices are detailed in Appendix A.

The jth harmonic order symmetric components of the mean and relative electric potentials are also interpolated linearly along the meridian

$$\left\{\varphi(s)\right\} = [N2(s)]\left\{\varphi^e\right\} \tag{5}$$

where

$$\langle\varphi\rangle = \langle\,\bar{\varphi}\quad\tilde{\varphi}\,\rangle,\ \langle\varphi^e\rangle = \langle\,\bar{\varphi}_1\quad\tilde{\varphi}_1\quad\bar{\varphi}_2\quad\tilde{\varphi}_2\,\rangle$$

Substituting this expression in those of the in-plane mean and relative, and transverse electric field components (Benjeddou et al., 2001), leads to

$$\left\{\bar{E}\right\} = [\bar{B}_\varphi]\left\{\bar{\varphi}^e\right\}, \quad \left\{\tilde{E}\right\} = [\tilde{B}_\varphi]\left\{\tilde{\varphi}^e\right\}, \quad E_z = \langle\hat{B}_\varphi\rangle\left\{\tilde{\varphi}^e\right\} \tag{6}$$

with

$$\langle\bar{E}\rangle = \langle\,\bar{E}_s\quad\bar{E}_\theta\,\rangle,\ \langle\tilde{E}\rangle = \langle\,\tilde{E}_s\quad\tilde{E}_\theta\,\rangle$$

$$\langle\varphi^e\rangle = \langle\,\bar{\varphi}_1\quad\bar{\varphi}_2\,\rangle,\ \langle\tilde{\varphi}^e\rangle = \langle\,\tilde{\varphi}_1\quad\tilde{\varphi}_2\,\rangle$$

The electric field matrices are also given in Appendix A.

DISCRETIZED EQUATIONS OF MOTION

Using discretized strains (4) and electric field (6) expressions, the internal mechanical, piezoelectric and electric virtual works are discretized in order to derive the sandwich shell stiffness matrix. Next, the inertia and external virtual works are also discretized in order to derive the mass matrix and load vector of the shell element. These discretized works are then substituted in the variational equation, described in Part 1 (Benjeddou et al., 2001) of the paper, in order to formulate the discretized equations of motion. The vibration problem is then derived for validation and application purpose.

Sandwich Shell Element Stiffness Matrix

The element stiffness matrix $[k]$ of the adaptive sandwich shell is obtained from the discretization of the internal virtual work

$$\delta W_{\text{int}} = \langle \delta d^e \rangle [k] \{d^e\} \tag{7}$$

where

$$\langle d^e \rangle = \langle\, \bar{u}_1 \quad \bar{v}_1 \quad w_1 \quad \bar{\beta}_1 \quad \bar{\beta}_{\theta 1} \quad \bar{\varphi}_1 \quad \tilde{u}_1 \quad \tilde{v}_1 \quad \tilde{\beta}_1 \quad \tilde{\beta}_{\theta 1} \quad \tilde{\varphi}_1 \quad \ldots \bar{u}_2 \quad \bar{v}_2 \quad w_2 \quad \bar{\beta}_2 \quad \bar{\beta}_{\theta 2} \quad \bar{\varphi}_2 \quad \tilde{u}_2 \quad \tilde{v}_2 \quad \tilde{\beta}_2 \quad \tilde{\beta}_{\theta 2} \quad \tilde{\varphi}_2 \,\rangle$$

Following the decomposition, made in part 1 (Benjeddou et al. 2001), of the internal virtual work into mechanical (m), piezoelectric (p) and electric (e) contributions, the element stiffness matrix of Equation (7) can be written in the form

$$[k] = [k^m] - [k^p] - [k^e] \tag{8}$$

where, the mechanical, piezoelectric and electric stiffness matrices are obtained from the following separate discretizations of the corresponding virtual works.

MECHANICAL STIFFNESS MATRIX

According to the decomposition, made in part 1 (Benjeddou et al. 2001) of the mechanical internal virtual work into extension (e), extension-bending ($e\chi$), bending (χ) and shear (γ) contributions, the mechanical stiffness matrix can be written as

$$[k^m] = [k_e^m] + [k_{e\chi}^m] + [k_\chi^m] + [k_\gamma^m] \tag{9}$$

where the extension, extension-bending, bending and shear stiffness matrices are derived from the following separate discretizations of the corresponding mechanical internal virtual works. Hence, substitution of the discretized extension strains (4) in the expression of the extension mechanical virtual work (Benjeddou et al. 2001), leads to

$$\begin{aligned} \delta W_e^m = {} & \langle \delta \bar{d}_t^e \rangle [\bar{k}_e] \{\bar{d}_t^e\} + \langle \delta \bar{d}_t^e \rangle [\tilde{\bar{k}}_e] \{\tilde{d}_p^e\} \\ & \langle \delta \tilde{d}_p^e \rangle [\tilde{\bar{k}}_e]^T \{\bar{d}_t^e\} + \langle \delta \tilde{d}_p^e \rangle [\tilde{k}_e] \{\tilde{d}_p^e\} \end{aligned} \tag{10}$$

The mean, mean-relative and relative extension mechanical stiffness matrices are detailed in Appendix B. Their assembly, according to the whole element DOF vector $\langle d^e \rangle$ of Equation (7) provides the extension mechanical stiffness matrix of Equation (9). Similarly, using the discretized expressions of the extension and bending strains (4) in the extension-bending mechanical virtual work equation (Benjeddou et al., 2001) gives

$$\begin{aligned} \delta W_{e\chi}^m = {} & \langle \delta \bar{d}_t^e \rangle [\bar{k}_{e\chi}] \{\bar{d}_r^e\} + \langle \delta \bar{d}_r^e \rangle [\bar{k}_{e\chi}]^T \{\bar{d}_t^e\} \\ & \langle \delta \bar{d}_t^e \rangle [\tilde{\bar{k}}_{e\chi}] \{\tilde{d}_r^e\} + \langle \delta \tilde{d}_r^e \rangle [\tilde{\bar{k}}_{e\chi}]^T \{\bar{d}_t^e\} \\ & \langle \delta \tilde{d}_p^e \rangle [\tilde{\bar{k}}_{\chi e}] \{\bar{d}_r^e\} + \langle \delta \bar{d}_r^e \rangle [\tilde{\bar{k}}_{\chi e}]^T \{\tilde{d}_p^e\} \\ & \langle \delta \tilde{d}_p^e \rangle [\tilde{k}_{e\chi}] \{\tilde{d}_r^e\} + \langle \delta \tilde{d}_r^e \rangle [\tilde{k}_{e\chi}]^T \{\tilde{d}_p^e\} \end{aligned} \tag{11}$$

The mean, mean-relative and relative extension-bending stiffness matrices are provided in Appendix B. Their assembly according to the element DOF vector $\langle d^e \rangle$ gives the extension-bending stiffness matrix in Equation (9). Also, combining the discretized equations of the bending strains (4) and the mechanical bending virtual work (Benjeddou et al., 2001), leads to

$$\begin{aligned} \delta W_\chi^m = {} & \langle \delta \bar{d}_r^e \rangle [\bar{k}_r] \{\bar{d}_r^e\} + \langle \delta \bar{d}_r^e \rangle [\tilde{\bar{k}}_\chi] \{\tilde{d}_r^e\} \\ & \langle \delta \tilde{d}_r^e \rangle [\tilde{\bar{k}}_\chi] \{\bar{d}_r^e\} + \langle \delta \tilde{d}_r^e \rangle [\tilde{k}_\chi] \{\tilde{d}_r^e\} \end{aligned} \tag{12}$$

where the mean, mean-relative and relative bending stiffness matrices are detailed in Appendix B. Again, their assembly according to the whole element DOF vector $\langle d^e \rangle$ provides the bending mechanical stiffness matrix in Equation (9). The discretization of the shear mechanical internal virtual work (Benjeddou et al., 2001) using the discretized shear strains (4), gives

$$\begin{aligned} \delta W_\gamma^m = {} & \langle \delta \bar{d}^e \rangle [\bar{k}_\gamma] \{\bar{d}^e\} + \langle \delta \bar{d}^e \rangle [\tilde{\bar{k}}_\gamma] \{\tilde{d}^e\} \\ & \langle \delta \tilde{d}^e \rangle [\tilde{\bar{k}}_\gamma]^T \{\bar{d}^e\} + \langle \delta \tilde{d}^e \rangle [\tilde{k}_\gamma] \{\tilde{d}^e\} \\ & \langle \delta \bar{d}^e \rangle [\bar{k}_\gamma^c] \{\bar{d}^e\} + \langle \delta \bar{d}^e \rangle [\tilde{\bar{k}}_\gamma^c] \{\tilde{d}^e\} \\ & \langle \delta \tilde{d}^e \rangle [\tilde{\bar{k}}_\gamma^c]^T \{\bar{d}^e\} + \langle \delta \tilde{d}^e \rangle [\tilde{k}_\gamma^c] \{\tilde{d}^e\} \end{aligned} \tag{13}$$

where the mean, mean-relative and relative shear stiffness matrices of the faces and the core are given in Appendix B. Their assembly in accordance to the element DOF vector $\langle d^e \rangle$ provides the shear mechanical stiffness matrix of Equation (9).

PIEZOELECTRIC STIFFNESS MATRIX

Following the decomposition, made in part 1 (Benjeddou et al., 2001), of the piezoelectric internal virtual work into extension, bending and shear contributions, the piezoelectric stiffness matrix is

$$[k^p] = [k^p_e] + [k^p_\chi] + [k^p_\gamma] \tag{14}$$

where the extension, bending and shear piezoelectric stiffness matrices are derived from the following separate discretization of the corresponding contributions to the piezoelectric internal virtual work. Hence, substituting the discretized extension strains (4) and in-plane electric field components (6) into the extension piezoelectric virtual work (Benjeddou et al., 2001) leads to

$$\begin{aligned}\delta W^p_e =& \langle \delta \bar{d}^e_t \rangle [\bar{k}^p_e] \{\bar{\varphi}^e\} + \langle \delta \bar{\varphi}^e \rangle [\bar{k}^p_e]^T \{\bar{d}^e_t\} \\ & \langle \delta \tilde{d}^e_p \rangle [\tilde{k}^p_e] \{\tilde{\varphi}^e\} + \langle \delta \tilde{\varphi}^e \rangle [\tilde{k}^p_e]^T \left\{\tilde{d}^e_p\right\}\end{aligned} \tag{15}$$

where the mean and relative extension piezoelectric stiffness matrices are given in Appendix B. Their assembly according to the element DOF vector $\langle d^e \rangle$ provides the extension piezoelectric stiffness matrix of Equation (14). In the same way, using the discretized bending strains and in-plane electric field components in the expression of the bending piezoelectric virtual work (Benjeddou et al., 2001) gives

$$\begin{aligned}\delta W^p_\chi =& \langle \delta \bar{d}^e_r \rangle [\bar{k}^p_\chi] \{\bar{\varphi}^e\} + \langle \delta \bar{\varphi}^e \rangle [\bar{k}^p_\chi]^T \{\bar{d}^e_r\} \\ & \langle \delta \bar{d}^e_r \rangle [\tilde{\bar{k}}^p_\chi] \{\tilde{\varphi}^e\} + \langle \delta \tilde{\varphi}^e \rangle [\tilde{\bar{k}}^p_\chi]^T \{\bar{d}^e_r\} \\ & \langle \delta \tilde{d}^e_r \rangle [\tilde{\bar{k}}^p_\chi] \{\tilde{\varphi}^e\} + \langle \delta \tilde{\varphi}^e \rangle [\tilde{\bar{k}}^p_\chi]^T \left\{\tilde{d}^e_r\right\} \\ & \langle \delta \tilde{d}^e_r \rangle [\tilde{k}^p_\chi] \{\tilde{\varphi}^e\} + \langle \delta \tilde{\varphi}^e \rangle [\tilde{k}^p_\chi]^T \left\{\tilde{d}^e_r\right\}\end{aligned} \tag{16}$$

where the mean, mean-relative, relative-mean and relative bending piezoelectric stiffness matrices are given in Appendix B. Their assembly using the element DOF vector $\langle d^e \rangle$ provides the bending piezoelectric matrix of Equation (14). Also, using the core shear strains (4), the shear contribution to the piezoelectric virtual work (Benjeddou et al., 2001) can be discretized as

$$\begin{aligned}\delta W^p_\gamma =& \langle \delta \bar{d}^e \rangle [\bar{k}^p_\gamma] \{\tilde{\varphi}^e\} + \langle \delta \tilde{\varphi}^e \rangle [\bar{k}^p_\gamma]^T \{\bar{d}^e\} \\ & \langle \delta \tilde{d}^e \rangle [\tilde{k}^p_\gamma] \{\tilde{\varphi}^e\} + \langle \delta \tilde{\varphi}^e \rangle [\tilde{k}^p_\gamma]^T \left\{\tilde{d}^e\right\}\end{aligned} \tag{17}$$

where, the mean and relative shear piezoelectric stiffness matrices are detailed in Appendix B. Their assembly using the element DOF vector $\langle d^e \rangle$ gives the shear contribution to the piezoelectric matrix of Equation (14).

ELECTRIC STIFFNESS MATRIX

Substituting the discretized electric field (6) into the electric internal virtual work gives

$$\begin{aligned}\delta W^e_{\text{int}} = & \langle \delta \bar{\varphi}^e \rangle [\bar{k}^e] \{\bar{\varphi}^e\} + \langle \delta \tilde{\varphi}^e \rangle [\tilde{k}^e] \{\tilde{\varphi}^e\} \\ & + \langle \delta \tilde{\varphi}^e \rangle [\hat{k}^e] \{\tilde{\varphi}^e\}\end{aligned} \tag{18}$$

mean and relative electric stiffness matrices are given in Appendix B. Their assembly, using the element DOF vector $\langle d^e \rangle$, provides the electric stiffness matrix of Equation (8).

Sandwich Shell Element Mass Matrix

The element mass matrix $[m]$ is derived from the discretization of the inertia virtual work

$$\delta W_{in} = \langle \delta d^e \rangle [m] \{d^e\} \tag{19}$$

Following the decomposition, made in Part 1 (Benjeddou et al. 2001), of the inertia virtual work into translation (u) translation-rotary ($u\beta$) and rotary (β) contributions, the element mass matrix is

$$[m] = [m_u] + [m_u \beta] + [m_\beta] \tag{20}$$

where translation, translation-rotary and rotary mass matrices are derived from the following separate discretization of the corresponding contributions of the inertia virtual work. Hence, the translation inertia virtual work can be discretized, using the displacement interpolations (3), as

$$\begin{aligned}\delta W_u =& \langle \delta \bar{d}^e_t \rangle [\bar{m}_u] \left\{\ddot{\bar{d}}^e_t\right\} + \langle \delta \tilde{d}^e_p \rangle [\tilde{\bar{m}}_u] \left\{\ddot{\tilde{d}}^e_p\right\} \\ & \langle \delta \tilde{d}^e_p \rangle [\tilde{\bar{m}}_u]^T \left\{\ddot{\bar{d}}^e_p\right\} + \langle \delta \tilde{d}^e_p \rangle [\tilde{m}_u] \left\{\ddot{\tilde{d}}^e_p\right\}\end{aligned} \tag{21}$$

where, the mean, mean-relative and relative translation mass matrices are given in Appendix C. Their assembly according to the element DOF vector $\langle d^e \rangle$, provides the translation mass matrix of Equation (20). Substituting the displacement and rotation interpolations (3) into the translation-rotary inertia virtual work (Benjeddou et al., 2001) leads to

$$\begin{aligned}\delta W_{u\beta} =& \langle \delta \bar{d}^e_p \rangle [\bar{m}_{u\beta}] \left\{\ddot{\bar{d}}^e_r\right\} + \langle \delta \bar{d}^e_r \rangle [\bar{m}_{u\beta}]^T \left\{\ddot{\bar{d}}^e_p\right\} \\ & \langle \delta \bar{d}^e_p \rangle [\tilde{\bar{m}}_{u\beta}] \left\{\ddot{\tilde{d}}^e_r\right\} + \langle \delta \tilde{d}^e_r \rangle [\tilde{\bar{m}}_{u\beta}]^T \left\{\ddot{\tilde{d}}^e_p\right\} \\ & \langle \delta \tilde{d}^e_p \rangle [\tilde{\bar{m}}_{\beta u}] \left\{\ddot{\bar{d}}^e_r\right\} + \langle \delta \bar{d}^e_r \rangle [\tilde{\bar{m}}_{\beta u}]^T \left\{\ddot{\tilde{d}}^e_p\right\} \\ & \langle \delta \tilde{d}^e_p \rangle [\tilde{m}_{u\beta}] \left\{\ddot{\tilde{d}}^e_r\right\} + \langle \delta \tilde{d}^e_r \rangle [\tilde{m}_{u\beta}]^T \left\{\ddot{\tilde{d}}^e_p\right\}\end{aligned} \tag{22}$$

where the mean, mean-relative and relative translation-rotary mass matrices are detailed in Appendix C. Their assembly, using the element DOF $\langle d^e \rangle$ gives the translation-rotary mass matrix of Equation (20). The use of the rotations interpolations (3) into the rotary inertia virtual work (Benjeddou et al., 2001) gives

$$\begin{aligned}\delta W_\beta = &\langle \delta \bar{d}_r^e \rangle [\bar{m}_\beta] \left\{ \ddot{\bar{d}}_r^e \right\} + \langle \delta \bar{d}_r^e \rangle [\tilde{\bar{m}}_\beta] \left\{ \ddot{\tilde{d}}_r^e \right\} \\ &\langle \delta \tilde{d}_r^e \rangle [\tilde{\bar{m}}_\beta]^T \left\{ \ddot{\bar{d}}_r^e \right\} + \langle \delta \tilde{d}_r^e \rangle [\tilde{m}_\beta] \left\{ \ddot{\tilde{d}}_r^e \right\}\end{aligned} \tag{23}$$

where, the mean, mean-relative and relative rotary mass matrices are given in Appendix C. Their assembly using the element DOF vector $\langle d^e \rangle$ leads to the rotary mass matrix in (20).

Sandwich Shell Element Mechanical Load Vector

The adaptive sandwich shell is assumed to be subjected to mechanical distributed (surface) and concentrated (line) loads, as detailed in part 1 (Benjeddou et al., 2001). Hence, the element load vector is obtained from the discretization of the mechanical external virtual work as

$$\delta W_{ext} = \langle \delta d^e \rangle \{f\} \tag{24}$$

where $\{f\}$ is the sum of the distributed, $\{f_d\}$, and concentrated, $\{f_c\}$, load contributions,

$$\{f\} = \{f_d\} + \{f_c\} \tag{25}$$

These are deduced from the following discretization of the corresponding virtual works. Hence, the distributed external virtual work (Benjeddou et al., 2001) can be discretized, using the displacement interpolations (3), as

$$\begin{aligned}\delta W_{ext}^d = &\langle \delta \bar{d}_t^e \rangle \left\{ \bar{f}_d^e \right\} + \langle \delta \bar{d}_r^e \rangle \left\{ \bar{m}_d^e \right\} \\ &\langle \delta \tilde{d}_p^e \rangle \left\{ \tilde{f}_d^e \right\} + \langle \delta \tilde{d}_r^e \rangle \left\{ \tilde{m}_d^e \right\}\end{aligned} \tag{26}$$

where the mean and relative distributed element forces and moments are detailed in Appendix D. The element nodal distributed load vector $\{f_d\}$ of Equation (25) is obtained by assembling these load vectors in accordance with the element DOF vectors $\langle d^e \rangle$. Similarly, the concentrated external virtual work (Benjeddou et al., 2001) can be discretized as

$$\begin{aligned}\delta W_{ext}^c = &\langle \delta \bar{d}_t^e \rangle \left\{ \bar{F}^e \right\} + \langle \delta \bar{d}_r^e \rangle \left\{ \bar{M}^e \right\} \\ &\langle \delta \tilde{d}_p^e \rangle \left\{ \tilde{F}^e \right\} + \langle \delta \tilde{d}_r^e \rangle \left\{ \tilde{M}^e \right\}\end{aligned} \tag{27}$$

where the mean and relative concentrated element forces and moments are given in Appendix D. Their assembly according to the element nodal DOF vector $\langle d^e \rangle$ leads to the concentrated element load vector $\{f_c\}$ of Equation (25).

Discretized Equations of Motion

All stiffness matrices are evaluated numerically using 2-point Gauss numerical integration rule. In fact, most functions to be integrated are rational with polynomial numerators and denominators of degrees 3 and 2, respectively. However, to avoid shear locking phenomenon, 1-point Gauss rule was used for the shear contributions. Thus, a maximum error of 2% has been obtained using 2-point Gauss integration for the membrane and bending contribution and 1-point rule for the shear ones. The mass matrices have been evaluated analytically as indicated in Appendix C.

Prior to their assembly, all above stiffness and mass matrices and load vectors, which were written in the local curvilinear coordinate system, should be transformed to the global cylindrical one in order to take into account the meridian curvature and its eventual geometric discontinuities. Hence, using the following relation, with $[P]$ the transformation matrix from the local curvilinear to the global cylindrical coordinate system

$$\{d^e\} = [P]\{D^e\} \tag{28}$$

the global element stiffness and mass matrices, and load vector can be obtained from the local ones by

$$\begin{aligned}&[K^e] = [P]^T[k][P], [M^e] = [P]^T[m][P] \\ &\{F^e\} = [P]^T\{f\}\end{aligned} \tag{29}$$

It is worthy to notice that the geometric transformation (28) augments the order of the matrices of Equation (29). Therefore, to avoid their singularities and in conformity with the through-thickness constant deflection assumption, the transformation-resulting relative deflection is constrained to vanish prior to their assembly.

Now, assembling these matrices in the frame of the d'Alembert variational Equation (Benjeddou et al., 2001), the discretized equations of motion can be written in the usual form

$$[M]\left\{\ddot{D}\right\} + [K]\{D\} = \{F\} \tag{30}$$

where $\{D\}$ is the global DOF vector including mechanical and electric DOF.

For validation purpose, the following harmonic eigenvalue problem with circular frequency ω is to be solved

$$\left(\begin{bmatrix} K_{uu} & K_{u\varphi} \\ K_{u\varphi}^T & K_{\varphi\varphi} \end{bmatrix} - \omega^2 \begin{bmatrix} M & 0 \\ 0 & 0 \end{bmatrix} \right) \begin{Bmatrix} q \\ \varphi \end{Bmatrix} = \begin{Bmatrix} 0 \\ 0 \end{Bmatrix} \tag{31}$$

where, the DOF vector $\{D\}$ of Equation (30) has been split into mechanical $\{q\}$ and electric$\{\varphi\}$ DOF subvectors. Prior to the solution of the previous system, the electric DOF are first condensed so that only the following reduced system is solved

$$\left([K_{uu} - K_{u\varphi}K_{\varphi\varphi}^{-1}K_{u\varphi}^{T}] - \omega^2[M]\right)\{q\} = \{0\} \qquad (32)$$

The condensed electric DOF can then be computed, *a posteriori*, using the relation

$$\{\varphi\} = -[K_{\varphi\varphi}K]^{-1}[K_{u\varphi}]^{T}\{q\} \qquad (33)$$

NUMERICAL VALIDATION

The present piezoelectric sandwich finite element has been first validated through comparison of its results with those obtained using an elastic sandwich one (Benjeddou and Hamdi, 1996). However, since the shear piezoelectric actuation mechanism is explored for the first time here, numerical reference values were not found in the open literature. Therefore, vibration of a short-circuited PZT-4 spherical shell is considered to check the validity of the present finite element implementation. The spherical symmetry involves well-known eigen frequencies multiplicity (Silbiger, 1962). That is, multiplicity is equal to the number of node lines on the sphere. Using a cylindrical coordinate system and Fourier series decomposition is expected to repeat fixed meridian index-frequencies (m) from the circumference index $j=0$ to the number of frequency multiplicity (Ohayon and Nicolas-Vullierme, 1981).

A PZT-4 piezoceramic spherical shell is now considered. Its material properties are: mass density $\rho = 7500\,\mathrm{Kg\,m^{-3}}$; elastic constants $C_{11} = 115\times10^{9}\mathrm{Nm^{-2}}$,$= C_{33} = 139\times10^{9}\mathrm{Nm^{-2}}$, $C_{12} = C_{13} = 74.3\times10^{9}\,\mathrm{Nm^{-2}}$, $C_{23} = 77.8\times10^{9}\,\mathrm{Nm^{-2}}$, $C_{44} = 30.6\times10^{9}\,\mathrm{Nm^{-2}}$, $C_{55} = C_{66} = 25.6\times10^{9}\,\mathrm{Nm^{-2}}$; piezoelectric constants $e_{11} = 15.1\,\mathrm{Cm^{-2}}$, $e_{12} = e_{13} = -5.2\,\mathrm{Cm^{-2}}$, $e_{35} = e_{26} = 12.7\,\mathrm{Cm^{-2}}$; dielectric constants $\varepsilon_{11} = \varepsilon_{12} = 1475\varepsilon_0$, $\varepsilon_{33} = 1300\varepsilon_0$, where the vacuum permittivity is $\varepsilon_0 = 8.854\times10^{-12}$ $\mathrm{Fm^{-1}}$. The shell is 0.5 mm thick and has a radius of 5 cm. The multiplicity repetitiveness of the eigen frequencies is checked through the error (relative difference) evaluation with respect to the axisymmetric ones ($j=0$). Results are presented in Table 1 for short-circuited ($\varphi=0$) electric boundary conditions on the inner and outer surfaces of the piezoceramic spherical shell.

It is clear from these results, that the above-mentioned spherical symmetry feature is well represented by the present simple conical piezoelectric sandwich finite element.

APPLICATIONS

After its validation, the present adaptive finite element is now used for vibrations analysis of some common axisymmetric shells. Hence, in the following, the modal characteristics are presented and electric boundary conditions effects are analyzed for hybrid sandwich simply supported (SS) cylinder and SS or clamped (C) circular plate with either short (SC)- or open (OC)-circuited shear actuators.

Vibrations of a Simply Supported Hybrid Sandwich Cylinder

Consider a SS sandwich cylinder with steel faces and piezoceramic (PZT-4) core. The latter is axially polarized and either SC or OC. The cylinder is relatively thick ($L/h=10$) and short ($L/R_{\mathrm{out}}=1$). Each face thickness is twice that of the core ($h_f/h_c=2$). Figure 2 shows the first six axisymmetric ($j=0$) modes of the hybrid sandwich cylinder.

This cylinder has been also analyzed for its conventional extension actuation mechanism (EAM) configuration. That is, with steel core and through-thickness polarized piezoceramic (PZT-4) faces (Gorge et al., 2001). Here the core thickness is twice that of each face in order to keep the same mass. Table 2 compares the first nine modes for both EAM and shear actuation mechanism (SAM) configurations. The piezoceramic layers are either SC or OC.

Table 1. Eigen frequencies (Hz) of a short-circuited PZT-4 spherical shell polarized along its meridian. Values in parentheses indicate errors (%) with respect to the axisymmetric values ($j=0$).

j	0	1	2	3	4	5	6	7
m								
1	3594	3597 (0.07)	3471 (−3.4)					
2	4327	4360 (0.8)	4241 (−2.0)	4115 (−4.9)				
3	4644	4700 (1.2)	4614 (−0.7)	4502 (−3.1)	4386 (−5.6)			
4	4843	4899 (1.2)	4849 (0.1)	4759 (−1.7)	4654 (−3.9)	4543 (−6.2)		
5	4999	5045 (0.9)	5025 (0.52)	4961 (−0.8)	4876 (−2.5)	4775 (−4.5)	4662 (−6.7)	
6	5133	5172 (0.8)	5180 (0.9)	5136 (0.05)	5077 (−1.1)	4996 (−2.7)	4891 (−4.7)	4773 (−7.0)

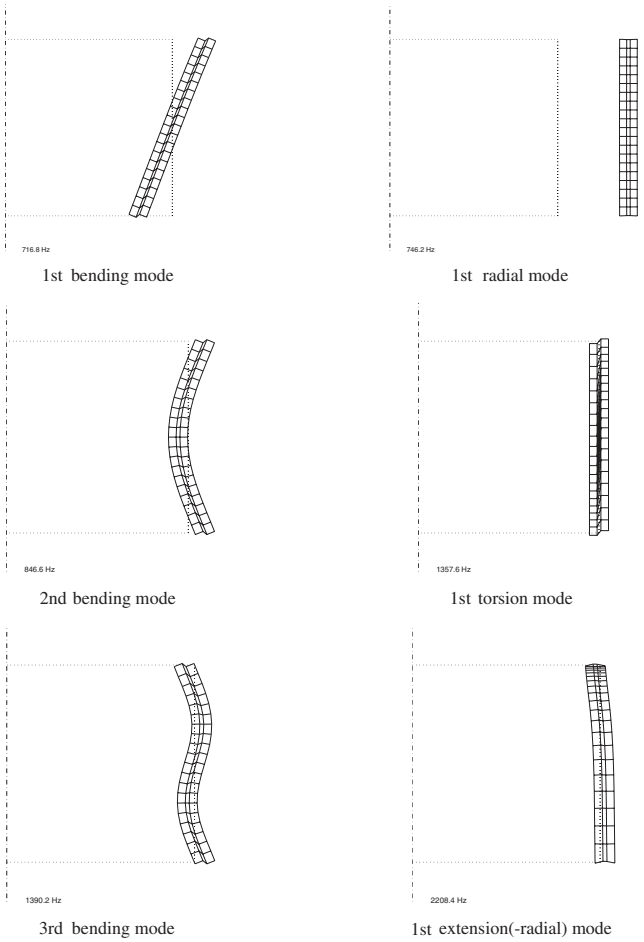

Figure 2. *First six axisymmetric modes of a SS, relatively thick and short hybrid sandwich cylinder.*

From Table 2, it is clear that shear actuators are insensitive to electric boundary conditions for their axisymmetric modes. This is also true for torsion modes with extension actuators, but not for their remaining axisymmetric modes. Table 2 also indicates that SAM leads to higher SC frequencies than EAM for all modes. This is due to the higher electromechanical coupling constants of the shear actuators (Benjeddou 2000b). Table 3 shows, for both electric boundary conditions, the first nine frequencies for $j = 1$–3.

In contrast to axisymmetric modes, Table 3 indicates that, for shear actuators, the non-axisymmetric bending modes depend on the electric boundary conditions and this dependence increases for higher modes. This is normal since for the latter, the transverse shear effect becomes more important. Therefore, for torsion and extension modes this dependence remains small. This can be explained by the fact that these modes are not electromechanically coupled for the shear actuation mechanism.

Vibrations of a Hybrid Sandwich Circular Plate

The modal characteristics of a SS or C hybrid sandwich circular plate of radius 0.6 m were analyzed by Wang et al. (2001) with EAM configuration. That is, with 1 mm-thick PZT-4 faces and 2 cm-thick steel core. Here, its equivalent SAM configuration is considered. The plate is then composed of a 2 mm-thick PZT-4 shear actuator sandwiched between two 1 cm-thick steel faces. The material properties are those used by Wang et al. (2001). The shear actuator is either short- or open-circuited in order to study the influence of the electric

Table 2. First nine axisymmetric frequencies of both EAM and SAM sandwich cylinder configurations.

Mode Type of mode		1 bending	2 radial	3 bending	4 torsion	5 bending	6 extension	7 bending	8 torsion	9 bending
EAM	OC	733.4	777	857.7	1266.4	1370.6	2160.8	2338.6	2541.1	3568.1
	SC	716.1	742.1	817	1266.4	1284.2	1991.8	2129.7	2541.1	3233.3
	(O-S)/S, %	2.42	4.03	4.98	0	6.73	8.48	9.81	0	10.35
SAM	S/OC	716.8	746.2	846.6	1357.6	1390.2	2208.4	2301.1	2723.4	3432.8
(SAM-EAM)/EAM	0.10	0.55	3.62	7.20	8.25	10.87	8.05	7.17	6.17	

Table 3. First nine frequencies for j = 1,2,3 of SAM sandwich cylinder with OC and SC configurations.

j	*m*	1	2	3	4	5	6	7	8	9
1	OC	646.48	710.43	853.23	1406.81	1583.06	2194.59	2318.49	2862.61	3448.00
	SC	646.48	710.35	852.65	1405.7	1583.03	2194.59	2317.11	2862.57	3446.52
	(O-S)/S, %	0	0.012	0.065	0.079	0.002	0	0.06	0.001	0.043
2	OC	513.88	697.77	892.99	1459.36	2047.63	2231.95	2370.59	3186.65	3493.44
	SC	513.76	697.38	890.73	1454.92	2047.60	2231.92	2365.07	3186.61	3487.51
	(O-S)/S, %	0.02	0.05	0.25	0.30	0.002	0.001	0.23	0.001	0.17
3	OC	455.62	700.92	969.08	1552.82	2371.37	2457.76	2598.18	3568.04	3602.66
	SC	454.95	699.66	963.76	1542.89	2371.29	2445.40	2598.15	3555.02	3602.34
	(O-S)/S, %	0.15	0.18	0.55	0.64	0.003	0.5	0.002	0.36	0.01

boundary conditions on the vibration behavior of the plate. The lowest four modes of the plate are given for both electric boundary conditions in Table 4 and in Figure 3 for the SS plate with OC shear actuator.

Table 4 confirms for both mechanical boundary conditions that with shear actuation, the OC frequencies are higher than SC ones, with nearly the same percent differences, and that the axisymmetric frequencies are insensitive to the electric boundary conditions.

A parametric analysis for various core (actuator) to faces thickness ratio ($h_c/2h_f$) was also made (Table 5) for the SS hybrid sandwich plate with OC shear actuator core. The core thickness was varied whereas that of the faces was kept constant. Notice that previous results correspond to the ratio 1/10 in Table 5. The latter indicates that the frequencies increase with increasing the core to faces thickness ratio. This tendency is similar to that obtained by Wang et al. (2001) for the same plate but with extension actuator.

Table 4. The lowest four frequencies of a SS or C plate with SC or OC shear actuator.

	Mode (*m,j*)	(1,0)	(1,1)	(1,2)	(2,0)
SS	OC	462.6	1298.9	2386.3	2783.4
	SC	462.6	1298.5	2384.3	2783.4
	100(O–S)/S, %	0	0.03	0.08	0
C	OC	952.18	1976.82	3233.71	3699.00
	SC	952.18	1976.30	3231.65	3699
	100(O–S)/S, %	0	0.026	0.06	0

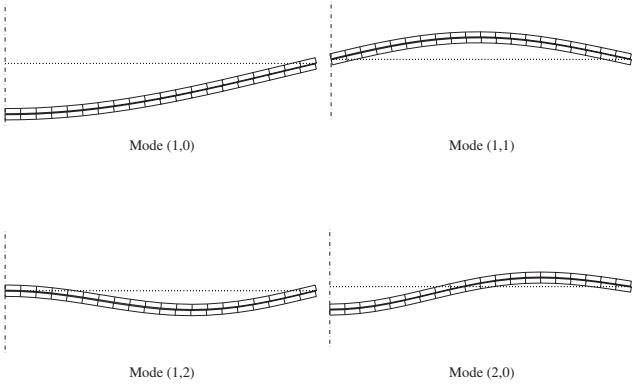

Figure 3. *The lowest four mode shapes of a SS circular plate ith OC shear actuator.*

Table 5. The lowest four frequencies of a SS plate with variable thickness OC shear actuator.

Mode (*m, j*)$h_c/2h_f$	(1,0)	(1,1)	(1,2)	(2,0)
1/12	455.5	1297.3	2350.7	2742.1
1/10	462.6	1298.9	2384.6	2783.4
1/8	473.2	1328.3	2439.5	2845.2
1/5	504.6	1415.4	2597.2	3028.3

CONCLUSION

A piezoelectric sandwich axisymmetric shell element has been implemented and validated in this second part of the paper (Benjeddou et al. 2001). It has the originality of using the shear mode of a piezoelectric core sandwiched between two elastic layers. The transverse shear response was explicitly represented through the faces relative tangential displacements DOF. Besides, the element has no derivative DOF since layer-wise shear deformation theory was retained for its formulation and linear Lagrange interpolations of all its independent variables were used for its implementation. This nice feature is particularly suitable for fluid-structure coupling analyses. Hence, the element formulation and implementation are being extended to axisymmetric shells filled with gas for structural-acoustic problems (interior noise reduction). Viscoelastic damping has also been considered for the core so that hybrid active-passive vibration control would be possible using the present finite element.

APPENDIX

A. Strain Matrices

The mean membrane strain matrix is

$$[B3]=\begin{bmatrix} -\frac{1}{L} & 0 & 0 & \frac{1}{L} & 0 & 0 \\ \frac{C}{r}N_1 & \frac{j}{r}N_1 & -\frac{S}{r}N_1 & \frac{C}{r}N_2 & \frac{j}{r}N_2 & -\frac{S}{r}N_2 \\ -\frac{j}{r}N_1 & -\frac{1}{L}-\frac{C}{r}N_1 & 0 & -\frac{j}{r}N_2 & \frac{1}{L}-\frac{C}{r}N_2 & 0 \end{bmatrix} \tag{A1}$$

where $C=\cos\psi_0$, $S=\sin\psi_0$, ψ_0 is defined in Figure 1. j is the circumference Fourier series index. N_1, N_2 are the linear shape functions defined in Equation (1). The relative membrane and bending strain matrix $[B2]$ is obtained from $[B3]$ by eliminating its 3rd and 6th columns.

The mean shear strain matrix of the faces has the following expression

$$[\bar{B}_s]=\begin{bmatrix} 0 & 0 & -\frac{1}{L} & N_1 & 0 & 0 & 0 & \frac{1}{L} & N_2 & 0 \\ 0 & \frac{S}{r}N_1 & -\frac{j}{r}N_1 & 0 & N_1 & 0 & \frac{S}{r}N_2 & -\frac{j}{r}N_2 & 0 & N_2 \end{bmatrix} \tag{A2}$$

The corresponding relative shear strain matrix is obtained from this matrix by suppressing its 3rd and 8th columns.

For the core, the above matrix can be written as

$$[\bar{B}_s^c] = \left[\begin{array}{cccccc|cccccc} 0 & 0 & -\frac{1}{L} & -\frac{\bar{h}}{h_c}N_1 & 0 & 0 & 0 & 0 & \frac{1}{L} & -\frac{\bar{h}}{h_c}N_2 & 0 & 0 \\ 0 & \frac{S}{r}N_1 & -\frac{j}{r}N_1 & 0 & -\left(\frac{\bar{h}}{h_c}+\frac{\tilde{h}}{4}\frac{S}{r}\right)N_1 & 0 & 0 & \frac{S}{r}N_2 & -\frac{j}{r}N_2 & 0 & -\left(\frac{\bar{h}}{h_c}+\frac{\tilde{h}}{4}\frac{S}{r}\right)N_2 \end{array}\right] \tag{A3}$$

The corresponding relative shear strain matrix is

$$[\tilde{B}_s^c] = \left[\begin{array}{cccc|cccc} \frac{N_1}{h_c} & 0 & -\frac{\tilde{h}}{4}\frac{N_1}{h_c} & 0 & \frac{N_2}{h_c} & 0 & -\frac{\tilde{h}}{4}\frac{N_2}{h_c} & 0 \\ 0 & \frac{N_1}{h_c} & 0 & -\frac{1}{4}\left(\frac{\tilde{h}}{h_c}+\bar{h}\frac{S}{r}\right)N_1 & 0 & \frac{N_2}{h_c} & 0 & -\frac{1}{4}\left(\frac{\tilde{h}}{h_c}+\bar{h}\frac{S}{r}\right)N_2 \end{array}\right] \tag{A4}$$

The mean and relative in-plane electric field matrix are, respectively

$$[\bar{B}_\varphi] = \begin{bmatrix} \frac{1}{L} & -\frac{1}{L} \\ \frac{j}{r}N_1 & \frac{j}{r}N_2 \end{bmatrix},\ [\tilde{B}_\varphi] = \frac{1}{h_c}[\bar{B}_\varphi] \tag{A5}$$

whereas, the transverse electric field line-vector is

$$\langle \hat{B}_\varphi \rangle = -\frac{1}{h_c}\langle\, N_1 \quad N_2 \,\rangle \tag{A6}$$

B. Stiffness Matrices

The mean, mean-relative and relative extension mechanical stiffness matrices are

$$\begin{aligned} [\bar{k}_e] &= \alpha\pi \int_0^L [B3]^T [\bar{D}_e][B3] r ds \\ [\bar{\tilde{k}}_e] &= \alpha\pi \int_0^L [B3]^T [\bar{\tilde{D}}_e][B2] r ds \\ [\tilde{k}_e] &= \alpha\pi \int_0^L [B2]^T [\tilde{D}_e][B2] r ds \end{aligned} \tag{B1}$$

where $\alpha = 1$ for $j = 0$ and $\alpha = 2$ otherwise.
The mean, mean-relative and relative extension-bending stiffness matrices are

$$\begin{aligned} [\bar{k}_{e\chi}] &= \alpha\pi \int_0^L [B3]^T [\bar{D}_{e\chi}][B2] r ds \\ [\bar{\tilde{k}}_{e\chi}] &= \alpha\pi \int_0^L [B3]^T [\bar{\tilde{D}}_{e\chi}][B2] r ds \\ [\bar{\tilde{k}}_{\chi e}] &= \alpha\pi \int_0^L [B2]^T [\bar{\tilde{D}}_{\chi e}][B2] r ds \\ [\tilde{k}_{e\chi}] &= \alpha\pi \int_0^L [B2]^T [\tilde{D}_{e\chi}][B2] r ds \end{aligned} \tag{B2}$$

The mean, mean-relative and relative bending mechanical stiffness matrices are

$$\begin{aligned} [\bar{k}_\chi] &= \alpha\pi \int_0^L [B2]^T [\bar{D}_\chi][B2] r ds \\ [\bar{\tilde{k}}_\chi] &= \alpha\pi \int_0^L [B2]^T [\bar{\tilde{D}}_\chi][B2] r ds \\ [\tilde{k}_\chi] &= \alpha\pi \int_0^L [B2]^T [\tilde{D}_\chi][B2] r ds \end{aligned} \tag{B3}$$

The mean, mean-relative and relative shear mechanical stiffness matrices of the faces are defined by

$$\begin{aligned} [\bar{k}_\gamma] &= \alpha\pi \int_0^L [\bar{B}_s]^T [\bar{D}_\gamma][\bar{B}_s] r ds \\ [\bar{\tilde{k}}_\gamma] &= \alpha\pi \int_0^L [\bar{B}_s]^T [\bar{\tilde{D}}_\gamma][\tilde{B}_s] r ds \\ [\tilde{k}_\gamma] &= \alpha\pi \int_0^L [\tilde{B}_s]^T [\tilde{D}_\gamma][\tilde{B}_s] r ds \end{aligned} \tag{B4}$$

whereas, those of the core are

$$\begin{aligned} [\bar{k}_\gamma^c] &= \alpha\pi \int_0^L [\bar{B}_s^c]^T [\bar{D}_\gamma^c][\bar{B}_s^c] r ds \\ [\bar{\tilde{k}}_\gamma^c] &= \alpha\pi \int_0^L [\bar{B}_s^c]^T [\bar{\tilde{D}}_\gamma^c][\tilde{B}_s^c] r ds \\ [\tilde{k}_\gamma^c] &= \alpha\pi \int_0^L [\tilde{B}_s^c]^T [\tilde{D}_\gamma^c][\tilde{B}_s^c] r ds \end{aligned} \tag{B5}$$

The mean and relative extension piezoelectric stiffness matrices are given by

$$\begin{aligned} [\bar{k}_e^p] &= \alpha\pi \int_0^L [\bar{B}_\varphi]^T [\bar{D}_e^p][B3] r ds \\ [\tilde{k}_e^p] &= \alpha\pi \int_0^L [\tilde{B}_\varphi]^T [\tilde{D}_e^p][B2] r ds \end{aligned} \tag{B6}$$

The mean, mean-relative, relative-mean and relative bending piezoelectric stiffness matrices are

$$
\begin{aligned}
[\bar{k}_{\chi}^{p}] &= \alpha\pi \int_0^L [B2]^T [\bar{D}_{\chi}^{p}][\bar{B}_{\varphi}] r ds \\
[\tilde{\bar{k}}_{\chi}^{p}] &= \alpha\pi \int_0^L [B2]^T [\tilde{\bar{D}}_{\chi}^{p}][\tilde{B}_{\varphi}] r ds \\
[\bar{\tilde{k}}_{\chi}^{p}] &= \alpha\pi \int_0^L [B2]^T [\bar{\tilde{D}}_{\chi}^{p}][\bar{B}_{\varphi}] r ds \\
[\tilde{k}_{\chi}^{p}] &= \alpha\pi \int_0^L [B2]^T [\tilde{D}_{\chi}^{p}][\tilde{B}_{\varphi}] r ds
\end{aligned}
\tag{B7}
$$

The mean and relative shear piezoelectric stiffness matrices have the form

$$
\begin{aligned}
[\bar{k}_{\gamma}^{p}] &= \alpha\pi \int_0^L [\bar{B}_{s}^{c}]^T \left\{ \bar{D}_{\gamma}^{p} \right\} \langle \hat{B}_{\varphi} \rangle r ds \\
[\tilde{k}_{\gamma}^{p}] &= \alpha\pi \int_0^L [\tilde{B}_{s}^{c}]^T \left\{ \tilde{D}_{\gamma}^{p} \right\} \langle \hat{B}_{\varphi} \rangle r ds
\end{aligned}
\tag{B8}
$$

The in-plane mean and relative, and transverse electric stiffness matrix are defined as

$$
\begin{aligned}
[\bar{k}^{e}] &= \alpha\pi \int_0^L [\bar{B}_{\varphi}]^T [\bar{\in}_{p}][\bar{B}_{\varphi}] r ds \\
[\tilde{k}^{e}] &= \alpha\pi \int_0^L [\tilde{B}_{\varphi}]^T [\bar{\in}_{p}][\tilde{B}_{\varphi}] r ds \\
[\hat{k}^{e}] &= \alpha\pi \int_0^L \left\{ \hat{B}_{\varphi} \right\} \bar{\in}_{zz} \langle \hat{B}_{\varphi} \rangle r ds
\end{aligned}
\tag{B9}
$$

C. Mass Matrices

The mean, mean-relative and relative translation mass matrices are defined by

$$
\begin{aligned}
[\bar{m}_{u}] &= \alpha\pi \int_0^L [N3]^T \bar{\rho}_{u} [N3] r ds \\
[\tilde{\bar{m}}_{u}] &= \alpha\pi \int_0^L [N2]^T \tilde{\bar{\rho}}_{u} [N2] r ds \\
[\tilde{m}_{u}] &= \alpha\pi \int_0^L [N2]^T \tilde{\rho}_{u} [N2] r ds
\end{aligned}
\tag{C1}
$$

where, $\alpha = 1$ for $j = 0$ and $\alpha = 2$ otherwise.

The mean, mean-relative, relative-mean and relative translation-rotary mass matrices are written as

$$
\begin{aligned}
[\bar{m}_{u\beta}] &= \alpha\pi \int_0^L [N2]^T \bar{\rho}_{u\beta} [N2] r ds \\
[\tilde{\bar{m}}_{u\beta}] &= \alpha\pi \int_0^L [N2]^T \tilde{\bar{\rho}}_{u\beta} [N2] r ds \\
[\tilde{\bar{m}}_{\beta u}] &= \alpha\pi \int_0^L [N2]^T \tilde{\bar{\rho}}_{\beta u} [N2] r ds \\
[\tilde{m}_{u\beta}] &= \alpha\pi \int_0^L [N2]^T \tilde{\rho}_{u\beta} [N2] r ds
\end{aligned}
\tag{C2}
$$

The mean, mean-relative and relative mass rotary matrices are given by

$$
\begin{aligned}
[\bar{m}_{\beta}] &= \alpha\pi \int_0^L [N2]^T \bar{\rho}_{\beta} [N2] r ds \\
[\tilde{\bar{m}}_{\beta}] &= \alpha\pi \int_0^L [N2]^T \tilde{\bar{\rho}}_{\beta} [N2] r ds \\
[\tilde{m}_{\beta}] &= \alpha\pi \int_0^L [N2]^T \tilde{\rho}_{\beta} [N2] r ds
\end{aligned}
\tag{C3}
$$

From Equations (C1–C3), notice that above mass matrices need computations of only two matrices which are

$$
\begin{aligned}
&\int_0^L [N3]^T [N3] r ds \\
&= \frac{L}{6} \begin{bmatrix}
r_1 + \bar{r} & 0 & 0 & \bar{r} & 0 & 0 \\
0 & r_1 + \bar{r} & 0 & 0 & \bar{r} & 0 \\
0 & 0 & r_1 + \bar{r} & 0 & 0 & \bar{r} \\
\bar{r} & 0 & 0 & r_2 + \bar{r} & 0 & 0 \\
0 & \bar{r} & 0 & 0 & r_2 + \bar{r} & 0 \\
0 & 0 & \bar{r} & 0 & 0 & r_2 + \bar{r}
\end{bmatrix}
\end{aligned}
\tag{C4}
$$

and $\int_0^L [N2]^T [N2] r ds$, which can be obtained from the previous matrix by omitting the 3rd and 6th lines and columns. $\bar{r} = (r_1 + r_2)/2$ is the mean radius of the element, where, r_1, r_2 are the polar radii of its two nodes.

D. Mechanical Load Vectors

The mean and relative applied distributed force and moment load vectors are

$$
\begin{aligned}
&\left\{ \bar{f}_{d}^{e} \right\} = \alpha\pi \int_0^L [N3]^T \left\{ \bar{f} \right\} r ds, \left\{ \tilde{f}_{d}^{e} \right\} = \alpha\pi \int_0^L [N2]^T \left\{ \tilde{f} \right\} r ds \\
&\left\{ \bar{m}_{d}^{e} \right\} = \alpha\pi \int_0^L [N2]^T \{ \bar{m} \} r ds, \left\{ \tilde{m}_{d}^{e} \right\} = \alpha\pi \int_0^L [N2]^T \{ \tilde{m} \} r ds
\end{aligned}
\tag{D1}
$$

At a point A with radial and axial coordinates (r_A, Z_A), the mean and relative applied concentrated force and moment load vectors can be written as

$$
\begin{aligned}
&\left\{ \bar{F}^{e} \right\} = \alpha\pi [N3(s_A)]^T \left\{ \bar{F} \right\} r_A, \left\{ \tilde{F}^{e} \right\} = \alpha\pi [N2(s_A)]^T \left\{ \tilde{F} \right\} r_A \\
&\left\{ \bar{M}^{e} \right\} = \alpha\pi [N2(s_A)]^T \left\{ \bar{M} \right\} r_A, \left\{ \tilde{M}^{e} \right\} = \alpha\pi [N2]^T \left\{ \tilde{M} \right\} r_A
\end{aligned}
\tag{D2}
$$

Where the applied loads in Equations (D1, D2) are either the symmetric or antisymmetric Fourier series components. Also, notice that s_A, in Equation (D2), is computed from the given coordinates (r_A, Z_A). Therefore, in practice, it is more easier to consider that

the concentrated loads are applied at the last node ($s_A = L$). Moreover, Equation (D2) can also be dropped in the implementation and the concentrated loads can simply be added, after the elements assembly, at the corresponding DOF of the nodes where they are applied.

REFERENCES

Benjeddou, A. (2000a). Advances in piezoelectric finite element modeling of adaptive Structural elements: a survey. *Comput. Struct.*, **76**: 347–363.

Benjeddou, A. (2000b). Piezoelectric transverse shear actuation of shells of revolution: theoretical formulation and analysis. *Europ. Congr. on Computational Methods in Appl. Sc. and Engng.* (*ECCOMAS*), Barcelona (Spain), (Invited Lecture).

Benjeddou, A., Gorge, V. and Ohayon, R. (2001). Use of piezoelectric shear response in adaptive sandwich shells of revolution–Part 1: theoretical formulation. *J. Intell. Mater. Syst. Struct.*, companion paper.

Benjeddou, A. and Hamdi, M.A. (1996). A B-Spline finite element for the dynamic analysis of sandwich shells of revolution. *Engng. Computations*, **13**: 241–264.

Gorge, V., Benjeddou, A. and Ohayon, R. (2001). Un élément fini pour le calcul des coques sandwich axisymétriques à peaux piézo-électriques. In: *5ème Colloque National en Calcul des Structures*, Giens (France), May 15–18.

Mackerle, J. (1998). Smart materials and structures-a finite element approach: a bibliography (1986–1997). *Modelling Simul. Sci. Eng.*, **6**: 293–334.

Ohayon, R. and Nicolas-Vullierme, B. (1981). An efficient shell finite element for the computation of the vibration of fluid structures systems of revolution. *Tech. Report* # 76, ONERA–Chatillon, France.

Saravanos, D.A. and Heyliger, P.R. (1999). Mechanics and computational models for laminated beams, plates and shells. *Appl. Mech. Rev.*, **52**: 305–320.

Silbiger, A. (1962). Non axisymmetric modes of vibration of thin spherical shells. *J. Acoust. Soc. Am.*, **34**: 362. (letter to the editor)

Wang, Q., Quek, S.T., Sun. and Liu, X. (2001). Analysis of piezoelectric coupled circular plate. *Smart Mater. Struct.*, **10**: 229–239.